ACCOUNTS of chemical research

pubs.acs.org/accounts Article

Biophysical Measurement Strategies for Antiviral Drug Development: Recent Progress in Virus-Mimetic Platforms Down to the Single Particle Level

Soohyun Park, Hyunhyuk Tae, and Nam-Joon Cho*

Cite This: *Acc. Chem. Res.* 2021, 54, 3204−3214 Read Online

CONSPECTUS: The rapid growth in the global human population has increased the prevalence of emerging infectious diseases, which poses a major risk to public health. In search of effective clinical solutions, the acquisition of knowledge and understanding of biomolecular processes associated with viral pathogens represents a prerequisite. In this context, biophysical engineering approaches are particularly promising since they can resolve biomolecular interactions systematically by circumventing the complexities associated with experiments involving natural biological systems. The engineering approaches encompass the design and construction of biomimetic platforms that simulate the physiological system. This approach enables us to characterize, measure, and quantitatively analyze biomolecular interactions.

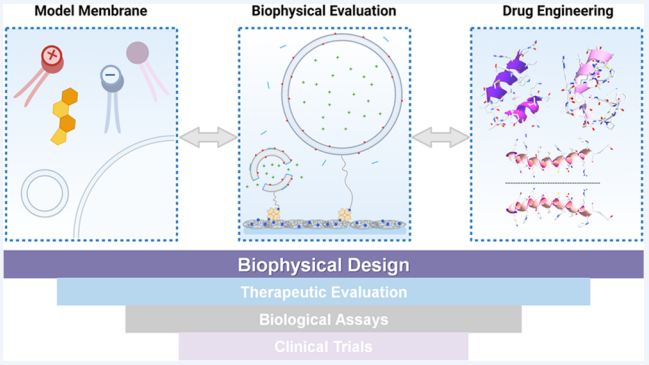

In this Account, we summarize biophysical measurements that our group has successfully adopted to develop broad-spectrum antiviral drugs based on the lipid envelope antiviral disruption (LEAD) strategy, targeting the structural integrity of the outer viral membrane to abrogate viral infectivity. We particularly focus on the engineering aspects related to the design and construction of the tethered lipid vesicle platform, which closely mimics the viral membrane. We first outline the development of the LEAD agents screening platform that integrates soft matter design components with biomaterials and surface functionalization strategies to facilitate parallel measurements tracking peptide-induced destabilization of nanoscale, virus-mimicking vesicles with tunable size and composition. Then, we describe how this platform can be effectively employed to gain insights into the membrane curvature dependency of certain peptides. The fundamental knowledge acquired through this systematic process is crucial in the identification and subsequent development of antiviral drug candidates. In particular, we highlight the development of curvature-sensitive α-helical (AH) peptides as a broad-spectrum antiviral agent that has been demonstrated as an effective therapeutic treatment against multiple enveloped viruses. Also, we introduce a tethered cluster of vesicles to mimic clusters of enveloped viruses, exhibiting higher infectivity levels in the biological system. Then, we discuss key considerations, including experimental artifacts, namely dye leakage and imaging-related photobleaching, and corresponding corrective measures to improve the accuracy of quantitative interpretation. With the ongoing development and application of the tethered lipid vesicle platform, there is a compelling opportunity to explore fundamental biointerfacial science and develop a new class of broad-spectrum antiviral agents to prepare for the future membrane-enveloped viral pandemics.

KEY REFERENCES

- Jackman, J. A.; Costa, V. V.; Park, S.; Real, A. L. C.; Park, J. H.; Cardozo, P. L.; Ferhan, A. R.; Olmo, I. G.; Moreira, T. P.; Bambirra, J. L.; Queiroz, V. F.; Queiroz-Junior, C. M.; Foureaux, G.; Souza, D. G.; Ribeiro, F. M.; Yoon, B. K.; Wynendaele, E.; Spiegeleer, B. D.; Teixeira, M. M.; Cho, N. J. Therapeutic treatment of Zika virus infection using a brain-penetrating antiviral peptide. *Nat. Mater.* **2018**, *17*, 971−977.[1] This paper describes the biophysical design and *in vivo* therapeutic effect of the engineered antiviral peptide against ZIKV infection through the lipid envelop antiviral disruption (LEAD) strategy.
- Park, S.; Jackman, J. A.; Cho, N. J. Comparing the membrane-interaction profiles of two antiviral peptides: insights into structure−function relationship. *Langmuir*

Received: May 16, 2021
Published: August 4, 2021

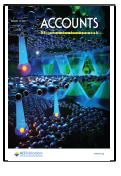

https://doi.org/10.1021/acs.accounts.1c00300
Acc. Chem. Res. 2021, 54, 3204−3214

Scheme 1. Representative History Map of Epidemics and Pandemics Caused by Lipid Membrane-Enveloped Viruses[a]

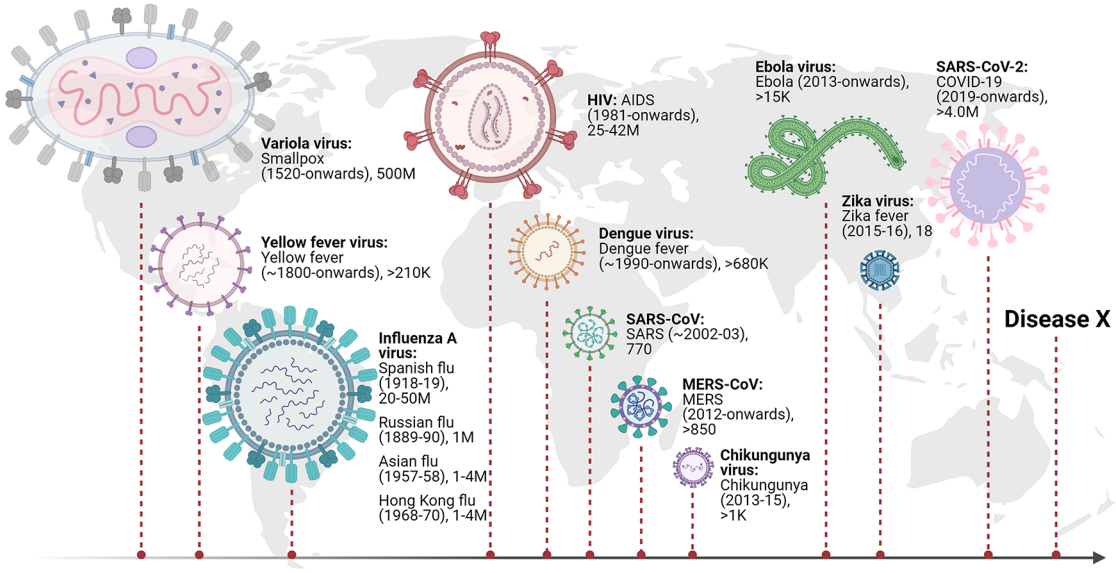

[a]Most of the viral pathogens that cause epidemic infectious diseases throughout history are lipid membrane-enveloped viruses, where variola viruses,[26] influenza viruses,[27,28] HIV,[29] Ebola virus, flaviviruses (dengue,[30] yellow fever,[31] and Zika[32] viruses), chikungunya virus,[33] and coronaviruses (MERS-CoV[34] and SARS-CoV-1[34] and 2[34,35]) are included. Disease X represents an unknown disease that could potentially cause the next pandemic. Each virus is presented by the virus type, disease, year(s), and estimated number of deaths.

2019, *35*, 9934−9943.[2] This paper utilizes multiple surface-sensitive measurement techniques along with a tethered lipid vesicle platform to investigate the membrane-interaction profiles of distinct antiviral peptides, providing insights into how peptides can be designed by connecting their conformational properties and activities.

- Park, S.; Jackman, J. A.; Xu, X.; Weiss, P. S.; Cho, N. J. Micropatterned viral membrane clusters for antiviral drug evaluation. *ACS Appl. Mater. Interfaces* **2019**, *11*, 13984−13990.[3] This paper demonstrates the virus-mimetic clusters of tethered vesicles assembled by micropatterning strategy.
- Tabaei, S. R.; Rabe, M.; Zhdanov, V. P.; Cho, N. J.; Höök, F. Single vesicle analysis reveals nanoscale membrane curvature selective pore formation in lipid membranes by an antiviral α-helical peptide. *Nano Lett.* **2012**, *12*, 5719−5725.[4] This paper first reports how AH peptide interacts with tethered phospholipid vesicles to induce membrane curvature dependent pore formation and derives a peptide-to-lipid ratio by the surface plasmon resonance (SPR) technique.

INTRODUCTION

As witnessed by the ongoing COVID-19 pandemic, the emergence of infectious diseases is a major public health concern that can lead to severe socioeconomic repercussions.[5] Especially, the rapid and heterogeneous transmission through the respiratory system has prolonged the COVID-19 pandemic for a long time,[6] resulting in significant constraints on livelihoods with impending huge economic costs. Although the race to achieve group immunization by the recently developed vaccine is underway,[7] experts predict it would take more than two years based on the current speed of immunization.[8,9] With the possibility of new waves of infectious diseases in the future, it is a timely opportunity to bring the attention of researchers across the biomedical sciences to the current progress in the development of biophysical engineering strategies that can be effectively employed to understand biomolecular processes relevant to infectious diseases.[10,11] To date, there already exists a substantial amount of work to prove that these strategies have yielded promising results in the identification of antiviral and antibacterial candidates.[1,12,13] Hence, by presenting this Account at this juncture, we hope that biophysical engineering strategies will receive broader reception within the scientific and clinical communities, accelerating existing efforts in combating emerging infectious diseases.

To prepare for the future pandemic,[14,15] we should recall the history of epidemics and pandemics. While most epidemic-causing viruses lack effective vaccines or therapies,[16,17] the majority of them have been caused by membrane-enveloped viruses, including variola viruses, influenza viruses, HIV, Ebola virus, flaviviruses (dengue, yellow fever, and Zika viruses), chikungunya virus, and coronaviruses (MERS-CoV, SARS-CoV-1 and 2) (Scheme 1). Although enveloped viruses might be more susceptible to the external environment, including humidity[18] or disinfectants[18,19] compared to nonenveloped ones, they feature other characteristics that could explain their high-profile outbreaks.[20] For example, the enveloped viruses exit from the host cell in the conventional secretion pathway (exocytosis) without cell damage and consequent immune responses. In contrast, nonenveloped viruses often cause host cell lysis.[21,22] Also, the lipid envelope functions as a cloak to hide the capsid antigens to avoid the host immune system.[23,24] Consequently, we predict that the possible future outbreaks caused by the unknown pathogen, or Disease X,[25] might be triggered by emerging or re-emerging membrane-enveloped viruses.

This Account focuses on a biophysical approach to develop broadly applicable antiviral drugs based on the lipid envelope antiviral disruption (LEAD) strategy,[1] targeting the structural

https://doi.org/10.1021/acs.accounts.1c00300
Acc. Chem. Res. 2021, 54, 3204−3214

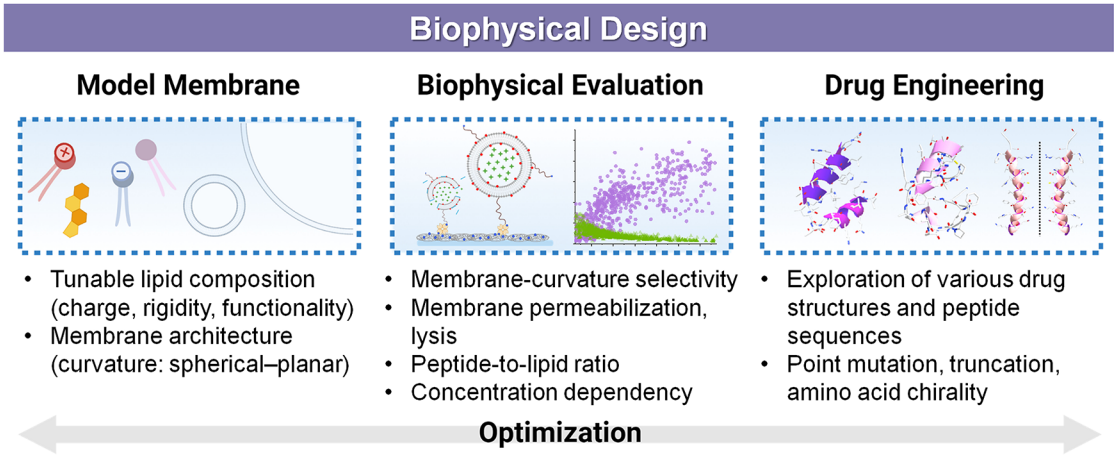

Figure 1. Overview of biophysical design concept to optimize the functionality of drug candidates. The model membrane platform enables tunable lipid compositions (charge, rigidity, and functionality) and membrane architecture to perform biophysical measurements that can assess the agent-induced membrane morphological change, curvature selectivity, concentration dependent activity, and peptide-to-lipid ratio. Based on the result, the drug can be engineered to optimize its targeted activity and undergo therapeutic evaluation, biological assays, and clinical trials.

integrity of the outer viral membrane to abrogate viral infectivity. Notably, the potential LEAD agents can be screened, evaluated, and optimized by virus-mimicking models or phospholipid vesicles (with combinations of other lipid compositions if necessary). We introduce how a tethered lipid vesicle platform provides insights to decipher the membrane curvature dependency of certain peptides in different aspects than other conventional screening assays such as surface-adsorbed or bulk suspension vesicles. Collectively, these efforts support that biointerfacial engineering strategies can be further refined and expanded to accelerate translational science research aimed at tackling the future emergence of infectious diseases.

BIOPHYSICAL MEASUREMENT STRATEGIES

A virus is an obligate intracellular parasite requiring the host cell machinery to replicate. The viral particle comprises a viral genome surrounded by a protein coat (capsid) and/or outer lipid membrane coating (envelope). The viral entry pathways of enveloped viruses involve membrane fusion between host cells and viruses, which is aided by the conformational change of spike proteins within the viral envelope.[36,37] As the capsid is physically separated from the envelope in general,[36] disruption of the structural integrity of the viral membrane eventually leads to the degradation of the viral capsid, including its genome, by exonucleases.[38] In addition, as protein receptors of the virus are found on the lipid envelope, the virus loses its virulence when the envelope is compromised.[39,40] This knowledge has been recently translated into the development of broadly applicable antiviral drugs based on the lipid envelope antiviral disruption (LEAD) strategy.[1]

The most important criteria of an antiviral drug candidate is to selectively target the virus particles while not harming the host cells. As the lipid compositions of host cell membranes and viral envelope membranes tend to be similar,[41] the selectivity from lipid compositions (e.g., differences in charge, rigidity, or fluidity) might be limited. Therefore, another approach has emerged from the difference in membrane curvature as the viral particles are ∼1000-fold smaller (<150 nm) than the usual host cell membranes (10−100 μm).

In analogy to the membrane coating of the virus, a similar diameter of lipid vesicle (enclosed lipid bilayer with aqueous compartment) can mimic the structural integrity of the virus. The extruded vesicles feature controlled size distribution and uniformity, which serve as an ideal platform for conducting biophysical measurements to engineer and evaluate drug candidates. The interaction between membrane-active agents and the model membrane can be scrutinized by tuning the membrane composition[32] (e.g., addition of charged lipids, functional molecules, or sterols) and architectural characteristics including membrane curvature.[42] Then, various biosensing techniques such as label-free acoustic/optical detection[13] or fluorescence microscopy[2] can be implemented to assess the agent-induced membrane morphological changes, destabilizing profiles, and curvature selectivity. These biophysical results and fundamental interpretations can guide the improvement of the drug candidate's selectivity, potency, toxicity, and stability. The overview of biophysical measurement strategies is presented in Figure 1.

WHY TETHERED LIPID VESICLE PLATFORM?

The illustration in Figure 2A describes how the lipid envelope antiviral disruption (LEAD) agents damage the lipid envelope and disintegrate the virus particle. As mentioned above, the association of LEAD agents with the lipid membrane surrounding enveloped virus impairs the infectivity of virus particles. Within this context, we highlight the two-fluorophore approach of the tethered lipid vesicle platform to track membrane permeabilization and membrane lysis simultaneously (Figure 2B).[4,43] The water-soluble dye, calcein (green), serves as an indicator of pore formation. In contrast, the headgroup-labeled phospholipid, Rh-PE (rhodamine PE, red), serves as a probe of membrane lysis. By biotin−neutravidin−biotin coupling, dually labeled vesicles are linked to a PLL-g-PEG-biotin coating at low surface coverage for monitoring with high spatial discrimination (Figure 2C). Upon adding a membrane-active agent at 0 min, the two types of membrane-interaction profiles can be real-time monitored using epifluorescence microscopy. While over 300 vesicles are captured per field of view, the fluorescence intensity (F.I.) changes of individual vesicles can be extracted and analyzed based on the experimental objectives.

While the method to extrude vesicles is widely documented,[42,44] the size distribution profile of lipid vesicles can be

https://doi.org/10.1021/acs.accounts.1c00300
Acc. Chem. Res. 2021, 54, 3204−3214

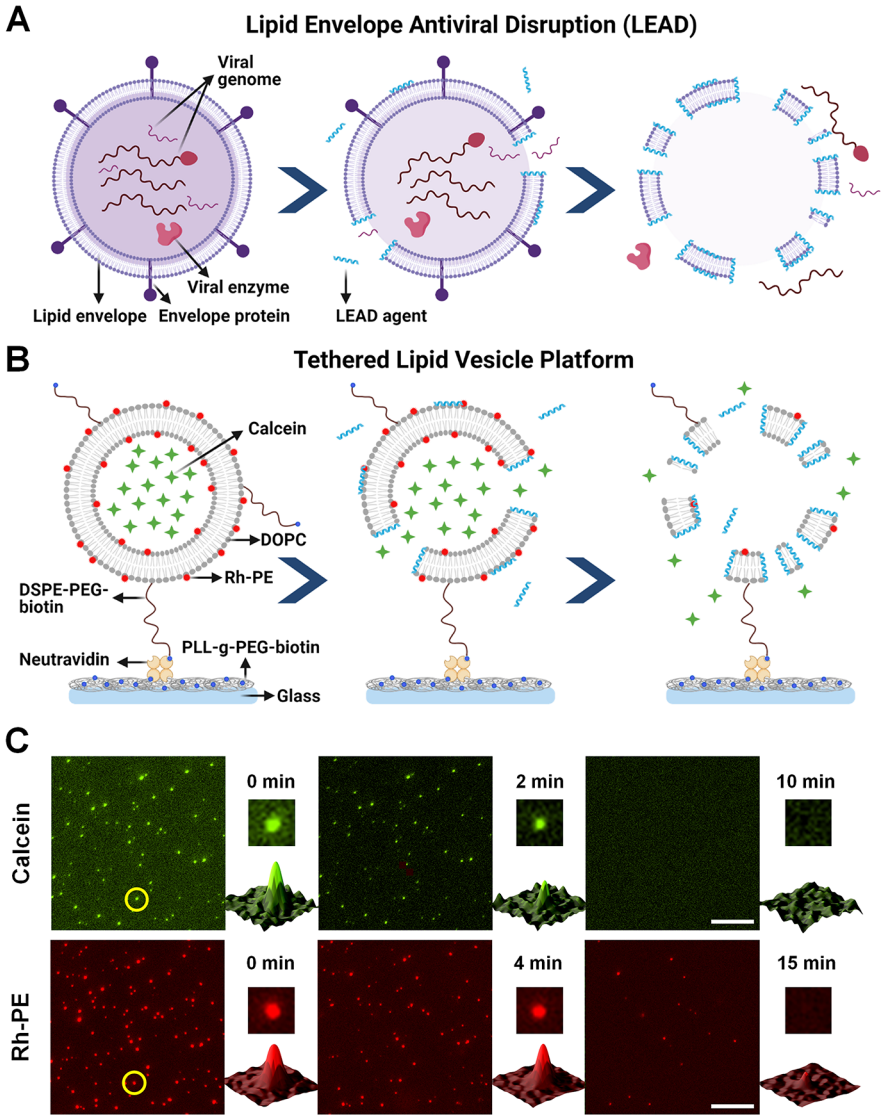

Figure 2. Lipid envelope antiviral disruption (LEAD) concept and tethered lipid vesicle platform mimicking virus particles. (A) Schematic illustration of the LEAD agent-induced virus particle's disintegration. (B) Schematic illustration of the two-probe tethered lipid vesicle platform for monitoring changes in membrane permeability (water-soluble calcein dye, green; encapsulated within lipid vesicles) and membrane rupture (rhodamine dye-labeled phospholipid (Rh-PE), red; in a vesicle's lipid bilayer). (C) Highly parallel measurement platform for single vesicle analysis. Time-lapse imaging is performed, and changes in fluorescence properties of individual vesicles can be analyzed. Scale bars are 20 μm.

characterized by cryogenic transmission electron microscopy (cryo-TEM) and static (SLS) or dynamic light scattering (DLS). Light scattering methods are the most commonly used techniques over others due to relatively simple sample preparation and the noninvasive characteristic.[45,46] Figure 3A shows the distribution of hydrodynamic diameter for vesicle populations extruded through different filter pore sizes of 50, 100, 200, and 400 nm. It should be noted that the larger pore size results in the broader distribution of vesicle diameter.[42]

There are numerous techniques to evaluate the effectiveness of vesicle lysis, including surface-sensitive measurements such as quartz crystal microbalance with dissipation (QCM-D). For example, QCM-D can monitor the total oscillating mass with coupled water and softness of the adhering layers by changing the resonance frequency and energy dissipation, respectively. In Figure 3B,[13] the decrease in frequency at 20−70 min indicates the vesicles are adsorbed on the sensor surface. Then, the added α-helical (AH) membrane-active peptide first binds to the adsorbed layer of vesicles as indicated by the decrease in the frequency (at 70 min), which is followed by the different degrees of increase in the frequency (loss of mass) depending on the size distribution of vesicles. Although this result shows that AH peptide less effectively ruptures the larger sizes of vesicles, the data interpretation for detailed kinetics involving simultaneous changes spanning multiple steps is challenging due to the convoluted signals of lipids and agents' mass (as well as viscoelasticity), accompanying dynamic events of membrane permeabilization, rupture, aggregation, and/or fusion.[47] Also, the surface-adsorbed vesicles tend to be deformed, and the vesicle−substrate interactions might influence the pathways.[13]

Alternatively, fluorescently labeled tethered vesicles provide precise information regarding the individual vesicle sizes and overcome the ensemble-averaged errors. Also, the multiprobe system enables the comprehensive measurement of membrane interactions including membrane permeabilization and lysis in a single-vesicle level. As can be seen in Figure 3C, the vesicles extruded through different pore sizes are tethered onto the

https://doi.org/10.1021/acs.accounts.1c00300
Acc. Chem. Res. 2021, 54, 3204−3214

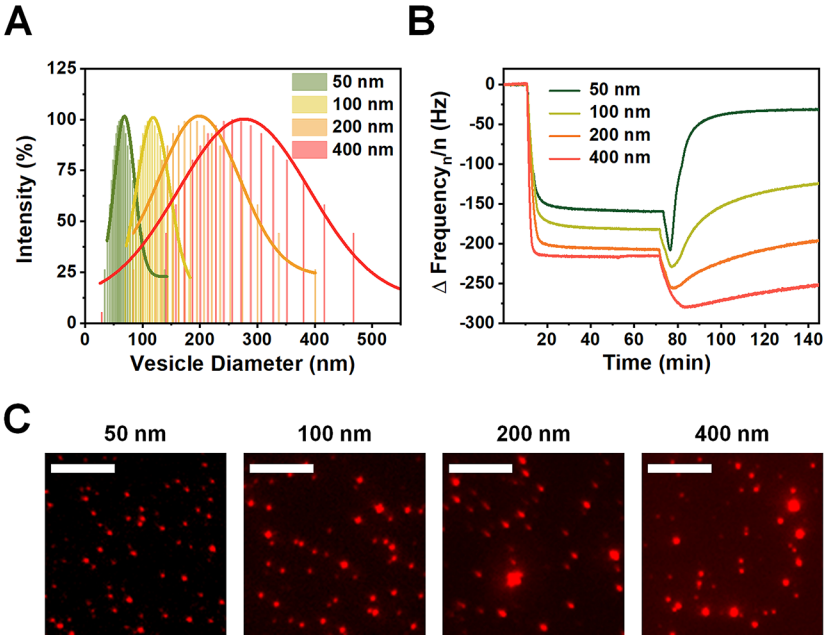

Figure 3. Size distribution of extruded vesicles compared ensemble-averaged quartz crystal microbalance with dissipation (QCM-D) and tethered vesicle monitoring. (A) Intensity weighted dynamic light scattering (DLS) data showing the size distribution (reported as hydrodynamic diameter) for vesicle populations with different filter sizes of 50, 100, 200, and 400 nm. (B) QCM-D frequency response for various vesicle size distributions upon AH peptide addition (vesicles added at ∼16 min; AH peptide added at ∼70 min). (C) Fluorescence microscopy images of tethered vesicles. The vesicle populations had different size distribution profiles depending on the extrusion processing conditions. Scale bars are 10 μm. Panel B is adapted with permission from ref 13. Copyright 2009 American Chemical Society. Panel C is adapted with permission from ref 1. Copyright 2018 Springer Nature.

surface, whereby thousands of individual lipid vesicles can be parallelly monitored using epifluorescence time-lapse imaging. Notably, the surface area of the individual vesicle is directly proportional to its fluorescent intensity (F.I.), which was originated from the surface-embedded fluorophores (Rh-PE). Therefore, the vesicle diameter ($D_{vesicle}$) is proportional to the square root of its F.I. ($\sqrt{F.I._{vesicle}}$), following the distribution of vesicle populations measured by DLS.[48] Overall, this relationship can be summarized by $D_{vesicle} = (\sqrt{F.I._{vesicle}}) \cdot \frac{D_{mean}}{(\sqrt{F.I.})_{mean}}$, whereby D_{mean} and $(\sqrt{F.I.})_{mean}$ denote the mean diameter of vesicles measured by DLS and the mean of the square root of the F.I. of tethered vesicles, respectively. Altogether, the tethered lipid vesicle platform provides not only time-resolved tracking of two-fluorophores indicating distinct membrane interactions but also their correlation with membrane curvatures (sizes), leading to further screening, evaluation, and optimization of the potential antiviral agents.

BIOPHYSICAL CHARACTERIZATION OF ANTIVIRAL AGENTS

Certain antiviral drugs, including specific amphipathic peptides, directly target the viral envelope and cause membrane destabilization, resulting in virus particle lysis and loss of infectivity. This class of membrane-active peptides is distinct from conventional antimicrobial peptides, whereby their net charges range from 0 to −2 or less. The most broadly studied two peptides are the 27-mer amphipathic, α-helix (AH) peptide and the 18-mer C5A peptide.[49] Both peptides are derived from the N-terminus of the hepatitis C virus (HCV) nonstructural protein 5A (NS5A), which plays an important role in HCV genome replication (Figure 4A). Although AH and C5A peptides share partially overlapping amino acid sequences due to their similar origin (HCV genotype 1b and 1a strain, respectively), their activity profiles have been known to be quite distinct. For example, it has been reported that the C5A peptide exhibits greater hemolytic activity than the AH peptide, showing less targeting selectivity.[50]

To screen and compare the activity profiles, both peptides were tested using the vesicles extruded through 100 and 400 nm filters.[2] For small vesicles (<125 nm diameter), 100 nM AH peptide ruptured the majority of vesicles within 12 min, while the same concentration of C5A peptide induced the rupture of vesicles within only 3 min (Figure 4B). On the other hand, only a minor fraction of vesicles was ruptured by 100 nM AH peptide for larger vesicles (>125 nm diameter), whereas 100 nM C5A peptide maintained its high activity toward larger ones comparable to the smaller ones. With a 10-fold lower concentration of 10 nM, C5A peptide preserved comparable activity while the membrane-disruptive activity of AH peptide was lost at the same concentration. Additionally, quantitative evaluation was performed by the final F.I. values of the Rh-PE signal per vesicle versus each of its sizes that was calculated from the corresponding initial F.I. (Figure 4C). The rupture efficiency of 100 nM AH peptide against small vesicles (>90%) was notably higher than the one against large vesicles (<20%). This preferential targeting ability was not observed from the 100 or 10 nM C5A peptide case, in which 100% of vesicles were ruptured regardless of the size of the vesicles.

Further investigation brought attention to the kinetic differences between the two peptides. In small vesicles, 100 nM AH peptide exhibited pore formation in ∼2 min, followed by membrane lysis within 5 min (Figure 4D). With larger vesicles, much slower permeabilization was observed without a noticeable change in Rh-PE signal, indicating AH peptide

https://doi.org/10.1021/acs.accounts.1c00300
Acc. Chem. Res. 2021, 54, 3204−3214

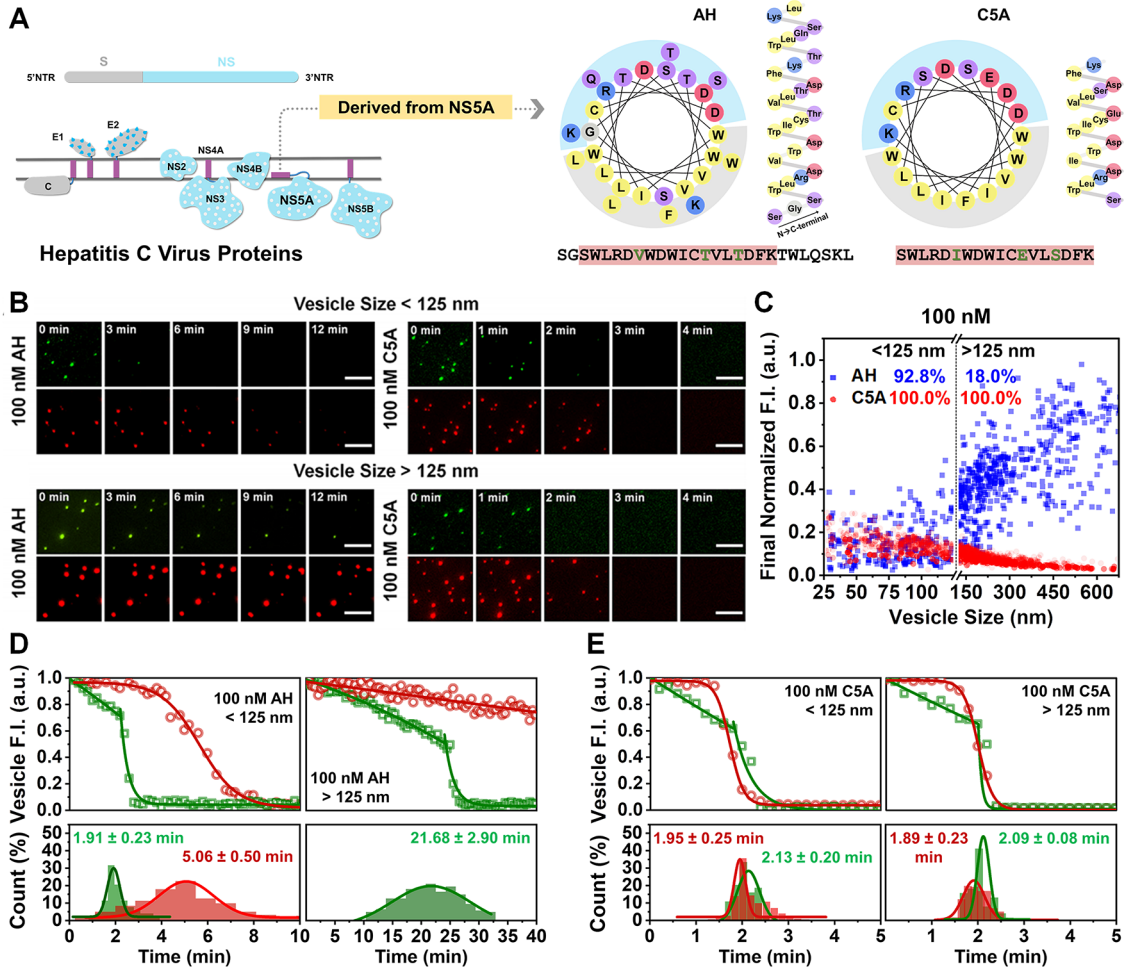

Figure 4. Biophysical characterization of LEAD agents. (A) Origin of tested peptides and their helical wheel projections: a 27-mer AH peptide and an 18-mer C5A peptide. (B) Time-lapse fluorescence microscopy images of encapsulated calcein (green, top) and Rh-PE (red, bottom) dye probes for the addition of 100 nM peptide to small vesicles (<125 nm diameter) and large vesicles (>125 nm diameter). Scale bars are 10 μm. (C) Corresponding single-vesicle data of peptide-induced vesicle rupture as a function of vesicle size, based on the rhodamine signal. (D and E) Change in normalized F.I. of individual, tethered vesicles as a result of membrane−peptide interactions. Top: Representative profiles of single-vesicle rupture kinetics for AH or C5A peptides at 100 nM for different vesicle size ranges. Green and red colors denote calcein and rhodamine signals, respectively. Bottom: Corresponding histogram statistics of membrane permeabilization (green) and membrane lysis (red) time scales where applicable. Adapted with permission from ref 2. Copyright 2019 American Chemical Society.

effectively forms pores only in small vesicles, and the membrane lysis occurs when a critical density of pores is reached. This observation coincides with our early study, which was conducted with a combination of tethered vesicles and surface plasmon resonance (SPR) technique to conclude that the membrane curvature (strain) dependent behavior of AH peptide is related to the pore formation (with extremely low peptide-to-lipid ratio) rather than the binding efficiency of the peptide.[4] Conversely, 100 nM C5A peptide induced membrane disruption within 2 min against all size ranges of vesicles (Figure 4E), manifesting the vesicle independent rupture activity with high potency. Particularly, in the C5A peptide, the time scale of membrane lysis was nearly equivalent to or even faster than the one required for membrane permeabilization, implying that its membrane-interaction profile is distinguished from that of AH peptide. Likewise, the tracking of single vesicle's F.I. changes can reveal the hidden interactions that are convoluted in ensemble-averaged measurements, especially focusing on the pore formation kinetics. These distinct membrane-disruptive activities between AH and C5A peptides are likely due to the conformational properties whereby C5A exhibits a larger coil-to-helix transition with lower free energy in the membrane environment.[2]

Further engineering efforts were built on enantiomers of AH peptide. While the above-mentioned AH peptides (unless otherwise specified) were composed of levorotary (L) amino acids (AH-L), dextrorotary (D) amino acids (AH-D) were investigated because D-isomeric forms tend to be more stable against degradation by proteases *in vivo* (higher bioavailability).[1] As a part of the biophysical characterization method, a tethered vesicle platform was used to compare the activity profiles of both peptides. Strikingly, the result indicated that the AH-D peptide exhibits more potent behavior than the AH-L peptide. The concentration dependent vesicle rupture profiles with rhodamine (Rh-PE) signals demonstrated that AH-D peptide induces more efficient and much quicker rupture of small vesicles starting from 50 nM than AH-L peptide (Figures 5A and B). At a high concentration of peptides (100 and 1000 nM), the trend was consistent, whereby the onset and complete rupture of vesicles induced by AH-D peptide was quicker than AH-L peptide. The

https://doi.org/10.1021/acs.accounts.1c00300
Acc. Chem. Res. 2021, 54, 3204−3214

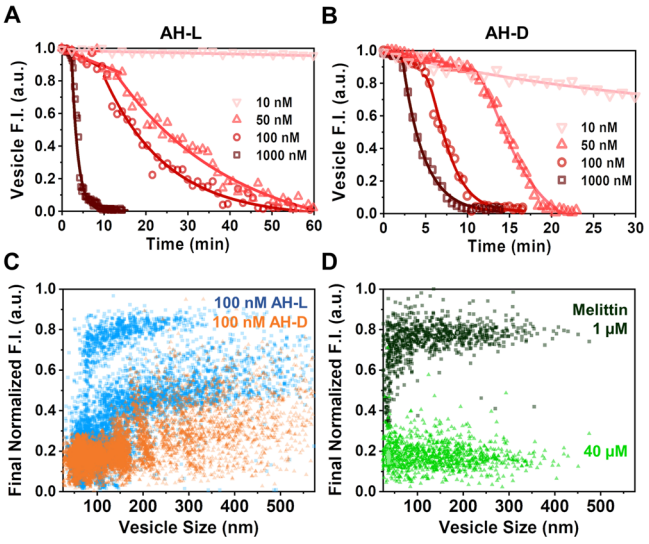

Figure 5. Biophysical design and characterization of AH peptide L- or D-enantiomers (referred to as AH-L and AH-D, respectively). Change in normalized F.I. of individual, tethered vesicles upon addition of 10, 50, 100, and 1000 nM of (A) AH-L and (B) AH-D. The profiles are selected from the vesicle diameter ranging ∼75 nm. Quantification of peptide-induced vesicle rupture as a function of vesicle diameter, where rupture is characterized by the final F.I. value of individual vesicles after treatment with (C) 100 nM AH-L or AH-D peptide and (D) 1 and 40 μM melittin peptide. Adapted with permission from ref 1. Copyright 2018 Springer Nature.

investigation on the effect of membrane curvature on the rupture efficiency (100 nM AH peptides) revealed that AH-L and AH-D have different preferential vesicle size ranges (Figure 5C). Although both peptides tend to target smaller vesicles, AH-L peptide mainly targeted vesicles below ∼125 nm while AH-D peptide showed a wider spectrum of ∼300 nm or less. On the other hand, melittin, a representative antimicrobial peptide, exhibited inactive (1 μM) or active (40 μM) behavior (Figure 5D), highlighting the unique behavior of both enantiomers of AH peptide. As introductions of D-diastereomers may affect the conformation and self-assembly behavior of peptides,[51] the biophysical performances and biological outcomes can be distinguished from their L-analogs, offering broader benefits beyond an enhancement of biostability. Collectively, this recent progress demonstrates that the several biophysical factors involved with amino acid sequences and/or their chirality affect the size dependent properties along with potencies, providing a deeper understanding of mechanistic details as well as opportunities to fine-tune the peptide's structure.

MIMICKING CLUSTERS OF ENVELOPED VIRUS PARTICLES

There has been an interest to develop clustered viral particles beyond single ones to reflect the biological relevance where the greater infectivity levels are observed among cooperative assemblies.[52] A hierarchically assembled cluster platform was fabricated by extending the previous single tethered vesicle platform using microcontact printing (μCP). The method starts from a poly(dimethylsiloxane) (PDMS) stamp with high precision to be later treated and covered with neutravidin, which is a linker to the biotinylated vesicles on a PLL-g-PEG-biotin-functionalized glass surface (Figure 6A). The patterned PDMS stamp was immersed with ink containing neutravidin of defined concentration for 5 min and dried by inert nitrogen gas. Then, neutravidin was printed onto the coated surface, whereby the specific attachment facilitates the high efficiency of transfer. For the high transfer success, it is noted that neutravidin should be printed within 1 min after drying. The subsequent addition of fluorescently labeled vesicles resulted in a higher level of patterned F.I. than the conventional, nonpatterned platform, indicating a successful clustered vesicle formation (Figure 6B). The patterned F.I. depended on the surface density of tethered vesicles; thus, the higher neutravidin concentration resulted in higher F.I. of clusters of vesicles. Notably, the μCP strategy required less reagent and incubation time than the nonpatterned platform because the direct transfer of neutravidin allowed overcoming diffusion-limited attachment.

Then, the effect of the antiviral AH peptide was evaluated using the micropatterned virus-mimetic clusters with varied neutravidin concentrations (vesicle densities) within individual clusters. The onset of pore formation (lag time) and the complete release of calcein were slower with the increasing neutravidin concentration, meaning that the peptide reaches by diffusion within clustered vesicles to cause membrane permeabilization with the highest cluster densities (Figures 6C and D). Then, membrane lysis was further investigated by tracking the F.I. changes of Rh-PE. Up to 10 μg/mL, the AH peptide caused complete lysis with a clear trend that the onset of membrane lysis (lag time) was more prolonged with the higher neutravidin concentration (Figure 6E and F). This also reflects that the small vesicles (<100 nm) maintained their physical structures within the cluster assembly. Incomplete lysis observed in 100 μg/mL suggests that the effectiveness of AH peptide might be limited when the system reaches specific vesicle densities. This proof-of-concept study can be further optimized to understand the physicochemical interactions of LEAD agents with viral clusters.

CONSIDERATIONS OF PHOTOBLEACHING AND DYE LEAKAGE

When the fluorescent dyes are subjected to repeated excitation−emission cycles such as time-lapse imaging with short time intervals and/or long duration, we should consider photobleaching effects involving the photochemical destruction of fluorophores. As most data interpretation assumes that the fluorescence signals are steady before adding any membrane-active compounds, there is a need to clarify the accumulative effect of photobleaching before starting sensitive measurements. Toward this goal, we introduce a systemic approach using time-lapse fluorescence microscopy in a tethered vesicle platform to identify the effect of imaging-related photobleaching and dye leakage involving different lipid compositions.[53] Generally, photobleaching is related to intrinsic dye properties and experimental conditions such as exposure frequency, exposure time, and excitation energy (light intensity). Among them, exposure time and excitation energy are set to be constant during a set of experiments. Therefore, for quantifying the photobleaching effect, the frequency of light exposure was controlled by the imaging (time) interval.

During simultaneous imaging of calcein and Rh-PE dyes, blue (494 nm) and green (560 nm) fluorescent light were used for excitation, inducing green (517 nm) and red (583 nm) light emissions, respectively. With defined imaging intervals of 0.4, 1, and 15 min, the increased frequency of light exposure

https://doi.org/10.1021/acs.accounts.1c00300
Acc. Chem. Res. 2021, 54, 3204−3214

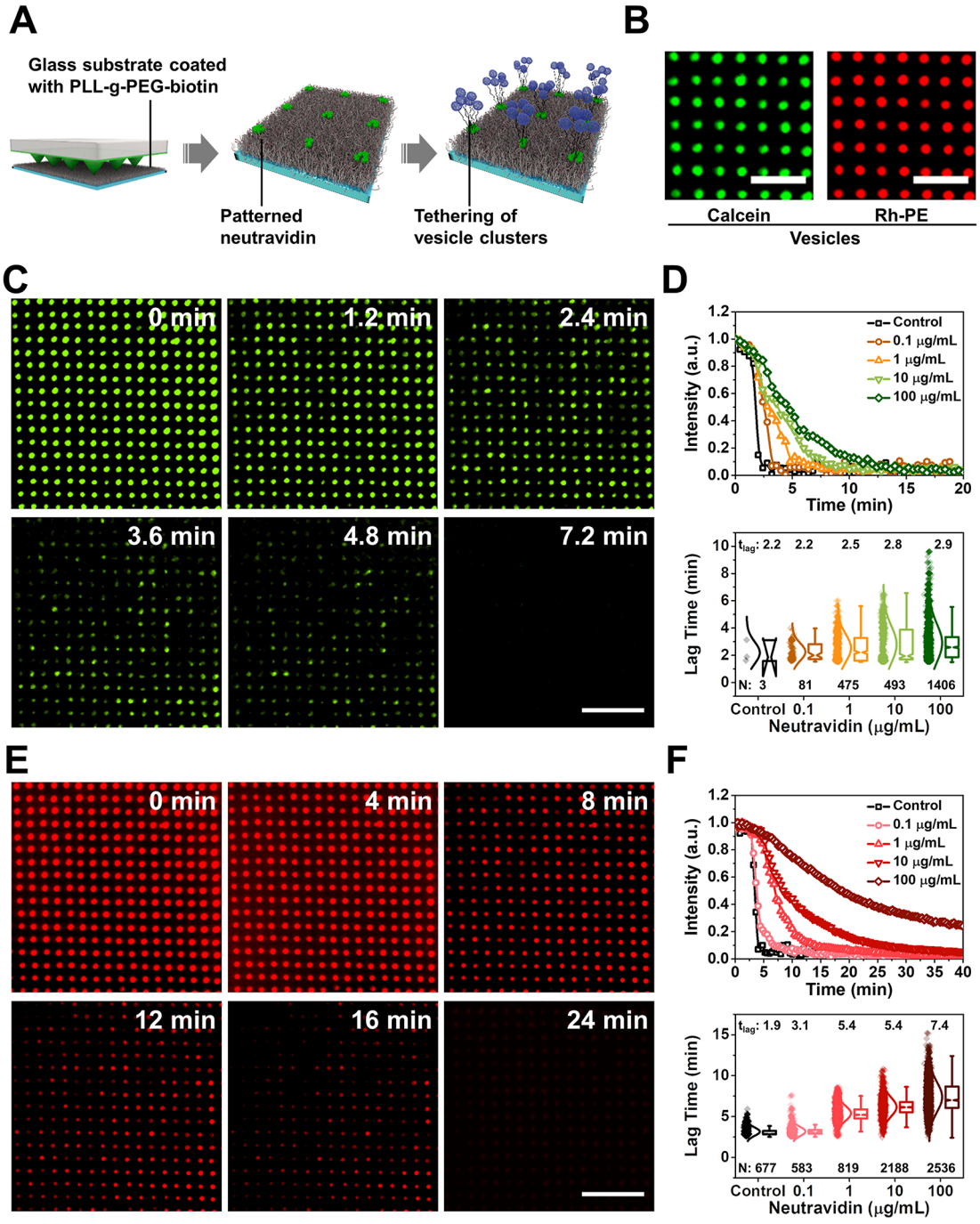

Figure 6. Design and characterization of the viral membrane cluster platform. (A) Schematic illustration describing the microcontact printing (μCP) strategy to form micropatterned viral membrane clusters. (B) Fluorescence microscope images of patterned vesicles on a PLL-g-PEG-biotin functionalized glass surface, as indicated by calcein and rhodamine signals. The scale bars are 10 μm. (C) Time-lapse fluorescent microscope images showing the change in calcein signal when 100 nM AH peptide was added to clusters at t = 0 min. During fabrication, the bulk neutravidin concentration was 10 μg/mL. (D) Top: Changes in the normalized calcein signal intensity of a representative, individual cluster for platforms fabricated using different neutravidin concentrations with the time-resolved release of the calcein marker. Bottom: Box plot graph reporting the trend in calcein release times. Each dot represents one cluster, and mean values are reported from Gaussian fitting. (E and F) Corresponding data are presented for the Rh-PE signal in the same experimental series. The scale bars are 20 μm. Control indicates the nonpatterned platform that was fabricated using a 10 μg/mL neutravidin concentration. Adapted with permission from ref 3. Copyright 2019 American Chemical Society.

(decreased imaging interval) caused a higher rate of calcein signal reduction (Figure 7A). On the contrary, the Rh-PE signal was largely stable throughout one hour of imaging (Figure 7B), suggesting that only the calcein signal is sensitive to photobleaching effects and needs further investigation. This also agrees with other studies showing that rhodamine based dyes have relatively higher photostability.[54]

Furthermore, different membrane compositions were investigated to evaluate the leakage of calcein dye. The selected lipids were anionic phospholipid (1,2-dioleoyl-sn-glycero-3-phospho-L-serine (sodium salt), DOPS) and choles-

https://doi.org/10.1021/acs.accounts.1c00300
Acc. Chem. Res. 2021, 54, 3204−3214

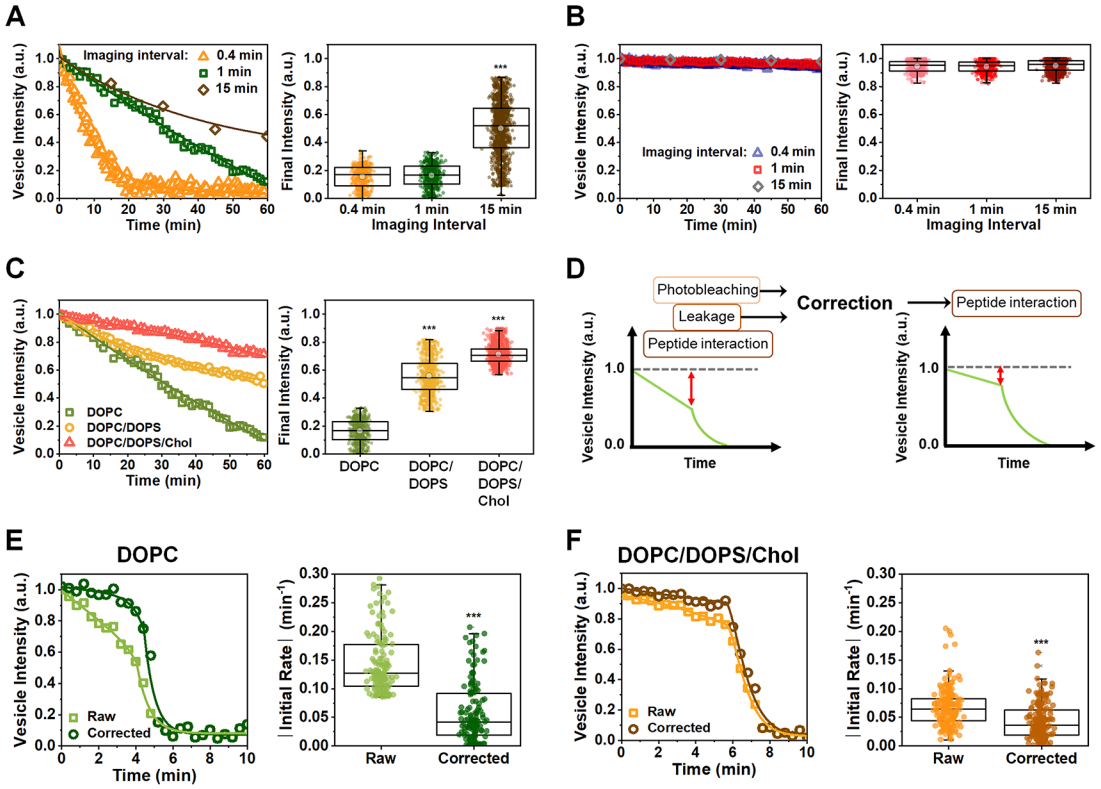

Figure 7. Characterization of the photobleaching and dye leakage effect from a two-probe tethered vesicle platform. Time-lapse changes (left) and statistical comparison (right) of the normalized fluorescence intensity of (A) calcein and (B) Rh-PE for different imaging intervals. (C) Time-lapse changes (left) and statistical comparison (right) of the normalized calcein intensity on different membrane compositions (DOPC, 100% DOPC; DOPC/DOPS, 92.5% DOPC/7.5% DOPS; DOPC/DOPS/Chol, 87.5% DOPC/7.5% DOPS/5.0% cholesterol) with a 1 min imaging interval. (D) Data normalization procedure to correct raw measurement data by removing the effects of dye photobleaching and nonspecific leakage. (E and F) Time-lapse plots (left) and quantification of the initial rate (right) of the change in the calcein intensity, with and without the correction procedure with a 0.4 min imaging interval upon the addition of 100 nM AH peptide. ***$P < 0.001$ compared to other groups by two-tailed t-tests. Adapted with permission from ref 53. Copyright 2019 Elsevier.

terol to compare the charge effect and membrane rigidity, respectively. The increased fraction of DOPS up to 7.5 mol % prevented the rapid decreasing rate of calcein (DOPC/DOPS in Figure 7C), supporting that the negative charge of DOPS hindered the leakage of calcein dye by electrostatic repulsion between the vesicle and anionic calcein dye. Also, the incorporation of cholesterol in the DOPC/DOPS vesicle showed significantly reduced leakage of calcein compared to the 100% DOPC case (DOPC/DOPS/Chol in Figure 7C) due to the reinforcement of packing between phospholipids.

Taken together, the data analysis involving a more extended observation period (time duration of the experiment) and/or different membrane compositions requires a data normalization procedure to correct for experimental artifacts. In other words, the photobleaching and dye leakage effect should be compensated using control experiments to avoid overestimation of a membrane-active compound's permeabilizing activity (Figure 7D). For instance, the initial rate of calcein's signal drop (raw data including the effect of pore formation, photobleaching, and leakage) caused by AH peptide is significantly higher (148% relative error) than the corrected data (Figure 7E). In contrast, much less discrepancy was obtained in DOPC/DOPS/Chol (Figure 7F). Likewise, the rate of pore formation differed up to 3-fold on various membrane compositions in the raw and corrective results. Therefore, considerations should be given to dye leakage, especially when the rate of different membrane compositions is compared. Of note, in the experimental settings with a relatively quick pore formation process (<10 min) with the same membrane compositions, the results can be directly compared without further correction processing unless the rate of pore formation should be quantified.

CONCLUSION

We have experienced multiple viral outbreaks, including the 2009 flu pandemic, Ebola, Zika, and COVID-19, which urged the global community to be prepared against emerging and re-emerging viruses. Conventional antiviral strategies based on biochemical principles, inhibiting the function of virus-specific components, are often limited to a certain range of viruses, and the error-prone viral genome quickly produces mutations, which complicates immediate responses.[37] However, many medically important viruses share a common feature of a membrane envelope that can provide the basis for a broad-spectrum antiviral targeting strategy. To this end, various viral membrane-related antiviral strategies have been investigated.[32] In this context, the biophysical engineering approaches are particularly promising because they can systematically resolve biomolecular interactions, avoiding the possible complexities of natural biological systems. Various combinatorial approaches of biosensing techniques and viral-membrane-mimicking platforms can lead to the efficient evaluation and rational design of drug candidates with broader merits. Among them, we focused on a multiprobe tethered lipid vesicle platform that

https://doi.org/10.1021/acs.accounts.1c00300
Acc. Chem. Res. 2021, 54, 3204−3214

grants interrogation of distinct key aspects such as membrane curvature selectivity and detailed kinetic insights at a single particle level. We envision these efforts detailed in this Account will pave the way to next-generation antiviral agents refined by fundamental knowledge acquired through biosensing techniques. With the ongoing efforts that LEAD agents can be safely administered intravenously in animal models,[1] there is excellent potential to translate the engineered drug molecules based on biophysical design to effective clinical solutions.

AUTHOR INFORMATION

Corresponding Author

Nam-Joon Cho − *School of Materials Science and Engineering, Nanyang Technological University, 639798, Singapore;* orcid.org/0000-0002-8692-8955; Email: njcho@ntu.edu.sg

Authors

Soohyun Park − *School of Materials Science and Engineering, Nanyang Technological University, 639798, Singapore;* orcid.org/0000-0003-3261-7585

Hyunhyuk Tae − *School of Materials Science and Engineering, Nanyang Technological University, 639798, Singapore;* orcid.org/0000-0002-0459-5879

Complete contact information is available at: https://pubs.acs.org/10.1021/acs.accounts.1c00300

Notes

The authors declare no competing financial interest.

Biographies

Soohyun Park received her B.S. in Biomaterials Engineering from Seoul National University in 2016 and Ph.D. in Materials Science and Engineering from Nanyang Technological University in 2021. She is currently conducting her postdoctoral research in the group of Professor Nam-Joon Cho at the School of Materials Science and Engineering, Nanyang Technological University. Her research interests involve antiviral peptides, model lipid membranes, and biomaterials.

Hyunhyuk Tae received his B.S. and M.S. in Biomaterials Engineering from Seoul National University in 2016 and 2018, respectively, after conducting graduate research under Professor Chang Seok Ki. He is currently a Ph.D. student in the group of Professor Nam-Joon Cho at the School of Materials Science and Engineering, Nanyang Technological University.

Nam-Joon Cho is a Professor in the School of Materials Science and Engineering at Nanyang Technological University. A recipient of the National Research Foundation Fellowship in Singapore, he received his Ph.D. in Chemical Engineering from Stanford University in 2007 January under the guidance of Professor Curtis W. Frank. After a postdoctoral fellowship at Stanford University School of Medicine working with Professor Jeffrey S. Glenn, he joined the faculty at Nanyang Technological University in 2011 as an associate professor. His research focuses on engineering artificial lipid membranes and lipid nanoparticle, biotechnology to tackle infectious diseases, and development of bioinspired materials.

ACKNOWLEDGMENTS

The authors thank all past and present members of the research group and the National Research Foundation of Singapore for a Competitive Research Programme grant (NRF-CRP10-2012-07). Scheme [1] and Figures [1] and [2]A and B were created with BioRender.com. The peptide structures from Figure [1] were aided by Swiss-PdbViewer 4.1.0.

REFERENCES

(1) Jackman, J. A.; Costa, V. V.; Park, S.; Real, A. L. C.; Park, J. H.; Cardozo, P. L.; Ferhan, A. R.; Olmo, I. G.; Moreira, T. P.; Bambirra, J. L.; Queiroz, V. F.; Queiroz-Junior, C. M.; Foureaux, G.; Souza, D. G.; Ribeiro, F. M.; Yoon, B. K.; Wynendaele, E.; Spiegeleer, B. D.; Teixeira, M. M.; Cho, N.-J. Therapeutic treatment of Zika virus infection using a brain-penetrating antiviral peptide. *Nat. Mater.* **2018**, *17*, 971−977.

(2) Park, S.; Jackman, J. A.; Cho, N.-J. Comparing the membrane-interaction profiles of two antiviral peptides: Insights into structure-function relationship. *Langmuir* **2019**, *35*, 9934−9943.

(3) Park, S.; Jackman, J. A.; Xu, X.; Weiss, P. S.; Cho, N.-J. Micropatterned viral membrane clusters for antiviral drug evaluation. *ACS Appl. Mater. Interfaces* **2019**, *11*, 13984−13990.

(4) Tabaei, S. R.; Rabe, M.; Zhdanov, V. P.; Cho, N.-J.; Höök, F. Single vesicle analysis reveals nanoscale membrane curvature selective pore formation in lipid membranes by an antiviral α-helical peptide. *Nano Lett.* **2012**, *12*, 5719−5725.

(5) Nicola, M.; Alsafi, Z.; Sohrabi, C.; Kerwan, A.; Al-Jabir, A.; Iosifidis, C.; Agha, M.; Agha, R. The socio-economic implications of the coronavirus and COVID-19 pandemic: a review. *Int. J. Surg.* **2020**, *78*, 185−193.

(6) Meyerowitz, E. A.; Richterman, A.; Gandhi, R. T.; Sax, P. E. Transmission of SARS-CoV-2: a review of viral, host, and environmental factors. *Ann. Intern. Med.* **2021**, *174*, 69−79.

(7) Kim, J. H.; Marks, F.; Clemens, J. D. Looking beyond COVID-19 vaccine phase 3 trials. *Nat. Med.* **2021**, *27*, 205−211.

(8) Rzymski, P.; Borkowski, L.; Drąg, M.; Flisiak, R.; Jemielity, J.; Krajewski, J.; Mastalerz-Migas, A.; Matyja, A.; Pyrć, K.; Simon, K. The strategies to support the COVID-19 vaccination with evidence-based communication and tackling misinformation. *Vaccines* **2021**, *9*, 109.

(9) Nkengasong, J. N.; Ndembi, N.; Tshangela, A.; Raji, T. COVID-19 vaccines: how to ensure Africa has access. *Nature* **2020**, *586*, 197−199.

(10) Cho, N.-J.; Glenn, J. S. Materials science approaches in the development of broad-spectrum antiviral therapies. *Nat. Mater.* **2020**, *19*, 1−4.

(11) Dolgin, E. The race for antiviral drugs to beat COVID-and the next pandemic. *Nature* **2021**, *592*, 340−343.

(12) Horvath, R.; Kobzi, B.; Keul, H.; Moeller, M.; Kiss, É. Molecular interaction of a new antibacterial polymer with a supported lipid bilayer measured by an in situ label-free optical technique. *Int. J. Mol. Sci.* **2013**, *14*, 9722−9736.

(13) Cho, N.-J.; Dvory-Sobol, H.; Xiong, A.; Cho, S. J.; Frank, C. W.; Glenn, J. S. Mechanism of an amphipathic alpha-helical peptide's antiviral activity involves size-dependent virus particle lysis. *ACS Chem. Biol.* **2009**, *4*, 1061−1067.

(14) Brady, O. J.; Hay, S. I. The global expansion of dengue: How Aedes aegypti mosquitoes enabled the first pandemic arbovirus. *Annu. Rev. Entomol.* **2020**, *65*, 191−208.

(15) Wilder-Smith, A.; Tissera, H.; Ooi, E. E.; Coloma, J.; Scott, T. W.; Gubler, D. J. Preventing dengue epidemics during the COVID-19 pandemic. *Am. J. Trop. Med. Hyg.* **2020**, *103*, 570−571.

(16) Diamond, M. S.; Pierson, T. C. The challenges of vaccine development against a new virus during a pandemic. *Cell Host Microbe* **2020**, *27*, 699−703.

(17) Ahmed, Q. A.; Memish, Z. A. Yellow fever from Angola and Congo: a storm gathers. *Trop. Doct.* **2017**, *47*, 92−96.

(18) Terpstra, F.; Van Den Blink, A.; Bos, L.; Boots, A.; Brinkhuis, F.; Gijsen, E.; Van Remmerden, Y.; Schuitemaker, H.; Van't Wout, A. Resistance of surface-dried virus to common disinfection procedures. *J. Hosp. Infect.* **2007**, *66*, 332−338.

(19) Howie, R.; Alfa, M.; Coombs, K. Survival of enveloped and non-enveloped viruses on surfaces compared with other micro-

organisms and impact of suboptimal disinfectant exposure. *J. Hosp. Infect.* **2008**, *69*, 368−376.
(20) Wisskirchen, K.; Lucifora, J.; Michler, T.; Protzer, U. New pharmacological strategies to fight enveloped viruses. *Trends Pharmacol. Sci.* **2014**, *35*, 470−478.
(21) Bird, S. W.; Kirkegaard, K. Escape of non-enveloped virus from intact cells. *Virology* **2015**, *479*, 444−449.
(22) Pornillos, O.; Garrus, J. E.; Sundquist, W. I. Mechanisms of enveloped RNA virus budding. *Trends Cell Biol.* **2002**, *12*, 569−579.
(23) Ngu, V. The viral envelope in the evolution of HIV: a hypothetical approach to inducing an effective immune response to the virus. *Med. Hypotheses* **1997**, *48*, 517−521.
(24) Feng, Z.; Lemon, S. M. Peek-a-boo: membrane hijacking and the pathogenesis of viral hepatitis. *Trends Microbiol.* **2014**, *22*, 59−64.
(25) Simpson, S.; Kaufmann, M. C.; Glozman, V.; Chakrabarti, A. Disease X: accelerating the development of medical countermeasures for the next pandemic. *Lancet Infect. Dis.* **2020**, *20*, 108−115.
(26) Henderson, D. A. *Smallpox: the death of a disease: the inside story of eradicating a worldwide killer*; Prometheus Books, 2009.
(27) *Pandemic influenza risk management: a WHO guide to inform and harmonize national and international pandemic preparedness and response*; World Health Organization, 2017.
(28) Shally-Jensen, M. *Encyclopedia of Contemporary American Social Issues [4 volumes]*; Abc-Clio, 2010.
(29) *Fact sheet - latest global and regional statistics on the status of the AIDS epidemic*; Joint United Nations Programme on HIV/AIDS: Geneva, 2020.
(30) Zeng, Z.; Zhan, J.; Chen, L.; Chen, H.; Cheng, S. Global, regional, and national dengue burden from 1990 to 2017: A systematic analysis based on the global burden of disease study 2017. *EClinicalMedicine* **2021**, *32*, 100712.
(31) Gaythorpe, K. A.; Hamlet, A.; Jean, K.; Ramos, D. G.; Cibrelus, L.; Garske, T.; Ferguson, N. The global burden of yellow fever. *eLife* **2021**, *10*, No. e64670.
(32) Yoon, B. K.; Jeon, W.-Y.; Sut, T. N.; Cho, N.-J.; Jackman, J. A. Stopping membrane-enveloped viruses with nanotechnology strategies: toward antiviral drug development and pandemic preparedness. *ACS Nano* **2021**, *15*, 125−148.
(33) Weaver, S. C.; Osorio, J. E.; Livengood, J. A.; Chen, R.; Stinchcomb, D. T. Chikungunya virus and prospects for a vaccine. *Expert Rev. Vaccines* **2012**, *11*, 1087−1101.
(34) Petersen, E.; Koopmans, M.; Go, U.; Hamer, D. H.; Petrosillo, N.; Castelli, F.; Storgaard, M.; Al Khalili, S.; Simonsen, L. Comparing SARS-CoV-2 with SARS-CoV and influenza pandemics. *Lancet Infect. Dis.* **2020**, *20*, 238−244.
(35) *WHO Covid-19 dashboard*; World Health Organization. http://covid19.who.int/ (accessed 2021-07-12).
(36) Lucas, W. Viral Capsids and Envelopes: Structure and Function. *Encyclopedia of Life Sciences (ELS)*; John Wiley & Sons, 2010.
(37) Komiyama, M. Molecular-Level Anatomy of SARS-CoV-2 for the Battle against the COVID-19 Pandemic. *Bull. Chem. Soc. Jpn.* **2021**, *94*, 1478−1490.
(38) Hanson, J. M.; Gettel, D. L.; Tabaei, S. R.; Jackman, J.; Kim, M. C.; Sasaki, D. Y.; Groves, J. T.; Liedberg, B.; Cho, N.-J.; Parikh, A. N. Cholesterol-enriched domain formation induced by viral-encoded, membrane-active amphipathic peptide. *Biophys. J.* **2016**, *110*, 176−187.
(39) Vigant, F.; Santos, N. C.; Lee, B. Broad-spectrum antivirals against viral fusion. *Nat. Rev. Microbiol.* **2015**, *13*, 426−437.
(40) Jackman, J. A.; Lee, J.; Cho, N. J. Nanomedicine for infectious disease applications: innovation towards broad-spectrum treatment of viral infections. *Small* **2016**, *12*, 1133−1139.
(41) Aloia, R. C.; Tian, H.; Jensen, F. C. Lipid composition and fluidity of the human immunodeficiency virus envelope and host cell plasma membranes. *Proc. Natl. Acad. Sci. U. S. A.* **1993**, *90*, 5181−5185.
(42) Jackman, J. A.; Zan, G. H.; Zhdanov, V. P.; Cho, N.-J. Rupture of lipid vesicles by a broad-spectrum antiviral peptide: influence of vesicle size. *J. Phys. Chem. B* **2013**, *117*, 16117−16128.
(43) Tabaei, S. R.; Cho, N. J. Lamellar sheet exfoliation of single lipid vesicles by a membrane-active peptide. *Chem. Commun.* **2015**, *51*, 10272−10275.
(44) Cho, N.-J.; Frank, C. W.; Kasemo, B.; Höök, F. Quartz crystal microbalance with dissipation monitoring of supported lipid bilayers on various substrates. *Nat. Protoc.* **2010**, *5*, 1096−1106.
(45) Dalgleish, D.; Hallett, F. Dynamic light scattering: applications to food systems. *Food Res. Int.* **1995**, *28*, 181−193.
(46) Hallett, F.; Watton, J.; Krygsman, P. Vesicle sizing: number distributions by dynamic light scattering. *Biophys. J.* **1991**, *59*, 357−362.
(47) Nir, S.; Nieva, J. L. Interactions of peptides with liposomes: pore formation and fusion. *Prog. Lipid Res.* **2000**, *39*, 181−206.
(48) Lohr, C.; Kunding, A. H.; Bhatia, V. K.; Stamou, D. Constructing size distributions of liposomes from single-object fluorescence measurements. *Methods Enzymol.* **2009**, *465*, 143−160.
(49) Cheng, G.; Montero, A.; Gastaminza, P.; Whitten-Bauer, C.; Wieland, S. F.; Isogawa, M.; Fredericksen, B.; Selvarajah, S.; Gallay, P. A.; Ghadiri, M. R.; Chisari, F. V. A virocidal amphipathic α-helical peptide that inhibits hepatitis C virus infection in vitro. *Proc. Natl. Acad. Sci. U. S. A.* **2008**, *105*, 3088−3093.
(50) Jackman, J. A.; Saravanan, R.; Zhang, Y.; Tabaei, S. R.; Cho, N. J. Correlation between membrane partitioning and functional activity in a single lipid vesicle assay establishes design guidelines for antiviral peptides. *Small* **2015**, *11*, 2372−2379.
(51) Chen, Y.; Mant, C. T.; Farmer, S. W.; Hancock, R. E.; Vasil, M. L.; Hodges, R. S. Rational design of α-helical antimicrobial peptides with enhanced activities and specificity/therapeutic index. *J. Biol. Chem.* **2005**, *280*, 12316−12329.
(52) Sanjuán, R. Collective properties of viral infectivity. *Curr. Opin. Virol.* **2018**, *33*, 1−6.
(53) Park, S.; Jackman, J. A.; Cho, N.-J. Quantitative accounting of dye leakage and photobleaching in single lipid vesicle measurements: implications for biomacromolecular interaction analysis. *Colloids Surf., B* **2019**, *182*, 110338.
(54) Soper, S. A.; Nutter, H. L.; Keller, R. A.; Davis, L. M.; Shera, E. B. The photophysical constants of several fluorescent dyes pertaining to ultrasensitive fluorescence spectroscopy. *Photochem. Photobiol.* **1993**, *57*, 972−977.

https://doi.org/10.1021/acs.accounts.1c00300
Acc. Chem. Res. 2021, 54, 3204−3214